Cumulative mixing inferred from stratospheric tracer relationships

Olaf Morgenstern,[1] Adrian M. Lee, and John A. Pyle
Centre for Atmospheric Science, Chemistry Department, Cambridge University, Cambridge, UK

Received 15 January 2001; revised 20 May 2002; accepted 25 June 2002; published 21 December 2002.

[1] Stratospheric mixing is studied using a chemical transport model simulating the evolution of 12 long-lived tracers at high resolution. A model integration is performed covering the period from March 1999 to August 2001. From the tracer relationships in the lower stratosphere we infer relative tracer lifetimes. Where the model captures the species' sinks properly and where the tracers are largely inert in the lower stratosphere, the model tracer lifetimes compare favorably with literature values. The breakup phases of the polar vortices in the two boreal winters covered by the simulation are studied in some detail. In both winters, before the final warming, separate canonical correlations appear. Mixing manifests itself in a progressive merger of the correlation curves marking the polar vortex and middle latitudes. We introduce a method to quantify the origins of fractions of simulated air masses based on tracer relationships describing the situation prior to the final warming. In both years, several weeks after the final vortex breakdown of the polar vortex, the method retrieves realistic quantities of former polar vortex air. The findings are verified using idealized tracer advection experiments. Some important differences between the two winters emerge with regard to the size and longevity of the polar vortex. *INDEX TERMS:* 0340 Atmospheric Composition and Structure: Middle atmosphere—composition and chemistry; 0341 Atmospheric Composition and Structure: Middle atmosphere—constituent transport and chemistry (3334); 3319 Meteorology and Atmospheric Dynamics: General circulation; 3334 Meteorology and Atmospheric Dynamics: Middle atmosphere dynamics (0341, 0342); *KEYWORDS:* mixing, stratosphere, tracer, long-lived, canonical, correlation

Citation: Morgenstern, O., A. M. Lee, and J. A. Pyle, Cumulative mixing inferred from stratospheric tracer relationships, *J. Geophys. Res.*, *107*, 8321, doi:10.1029/2002JD002098, 2002. [printed *108*(D5), 2003]

1. Introduction

[2] A common method to assess ozone depletion, denitrification, or dehydration in the stratosphere is to evaluate the effects of these processes on relationships with long-lived trace gases [e.g., *Kelly et al.*, 1989; *Proffitt et al.*, 1989, 1990; *Fahey et al.*, 1990; *Müller et al.*, 1996, 2001]. Strictly such an approach is valid only if mixing processes can be ignored; otherwise mixing needs to be quantified [*Rex et al.*, 1999; *Plumb et al.*, 2000]. Tracer correlations generally differ between different regions of the atmosphere separated by transport barriers [e.g., *Goldan et al.*, 1980; *Plumb*, 1996; *Murphy et al.*, 1993; *Michelsen et al.*, 1999; *Ray et al.*, 2002; *Piani et al.*, 2002], reflecting the different photochemical histories of air masses on either side of the transport barrier. Hence mixing across the vortex edge, for example, has the potential to change tracer relationships without chemistry having to be invoked.

[3] In spring upon the breakdown of the vortex, ozone depleted former vortex air is flushed into middle latitudes. Satellite measurements taken during the period 1979–1997 indicate that springtime ozone trends in middle latitudes are about −6% per decade [*World Meteorological Organization* (*WMO*), 1999]. Some authors, e.g., *Tuck et al.* [1992], *Pyle et al.* [1995], *Knudsen and Grooß* [2000], *Knudsen and Andersen* [2001], and *Millard et al.* [2002], have attributed much of this to enhanced ozone depletion in the polar vortex. Some chemical recovery of ozone depleted air is however conceivable, and the relative importance of mixing processes remains to be quantitatively understood. Moreover, details of the mixing processes vary strongly from year to year. Long-lived vortex fragments have been observed up to two months after vortex breakdown [e.g., *Hess*, 1991; *Newman et al.*, 1996].

[4] Attempts have been made to quantify the effects of mixing on a dynamical basis. *Minschwaner et al.* [1996], *Volk et al.* [1996], and *Avallone and Prather* [1996] consider the extent to which mixing with middle latitude air modifies the composition of the tropical stratosphere. *Minschwaner et al.* [1996] and *Volk et al.* [1996] compare measurements of long-lived tracers to the numerical solution of a simplified budget equation accounting for mean diabatic ascent, photochemistry, and mixing with midlatitude air. *Minschwaner et al.* [1996] discuss the origins of substantial uncertainties in their results, which are mainly due to uncertainties in the mean profiles and in mean diabatic heating. Their approach neglects seasonal effects, focussing on annual mean features. When applied to the polar vortex this simplification would no longer be possible

[1]Now at Max-Planck-Institut für Meteorologie, Hamburg, Germany.

0148-0227/02/2002JD002098

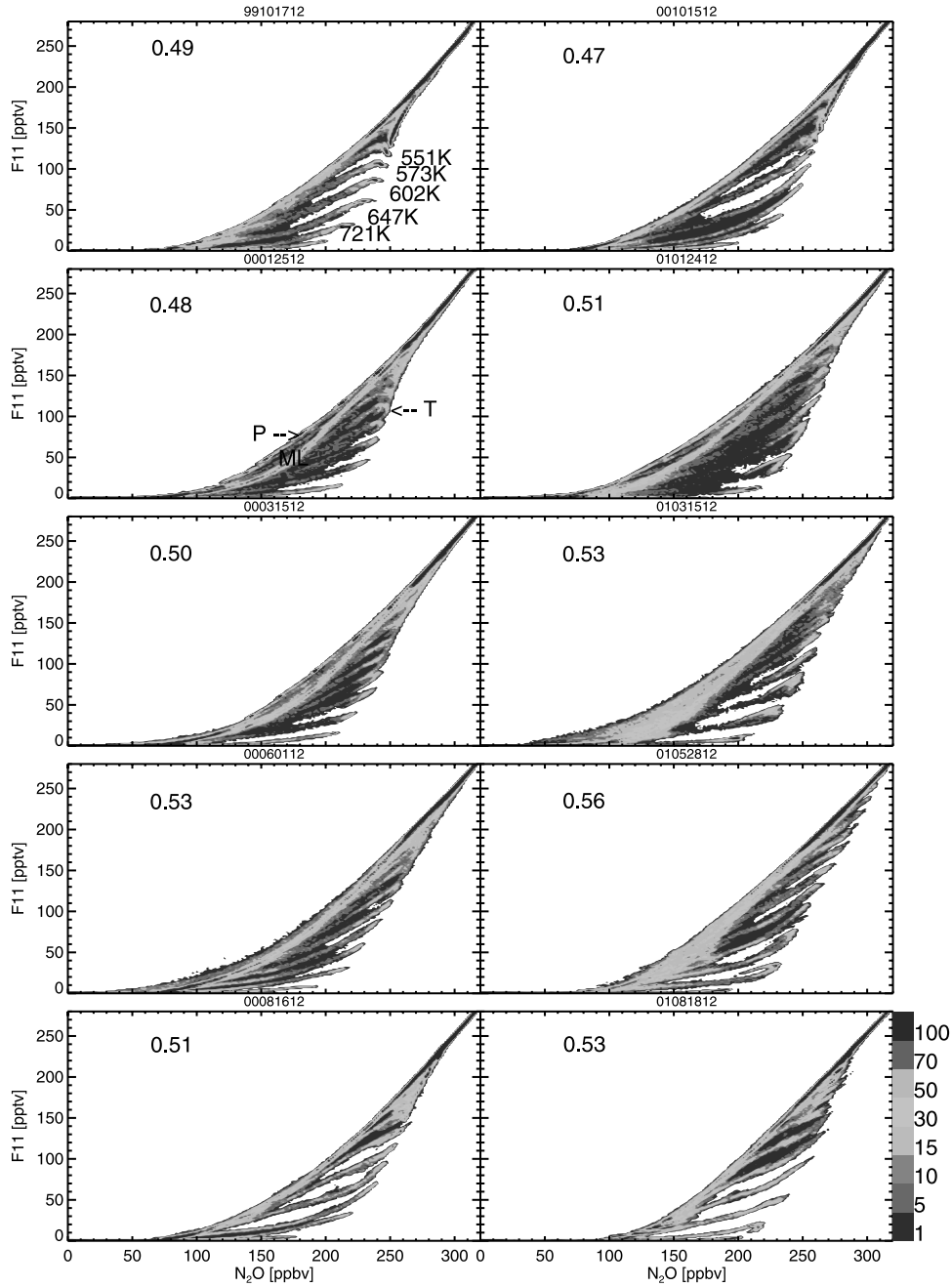

Figure 1. Density scatterplots of CFC-11 versus N_2O. Displayed dates are (left) 17 October 1999, 25 January, 15 March, 1 June and 16 August 2000; (right) 15 October 2000, 24 January, 15 March, 28 May, and 18 August 2001, all 1200 UTC. The displayed parameter space is divided into 200 × 200 equal-sized cells and the number of model grid points falling into each cell is counted. The bottom-boundary level at 350 K (362 K after July 2000) and Southern Hemisphere grid points are excluded. The numbers in the top left corners of the plots are $\tau_{CFC-11}/\tau_{N_2O}$, derived geometrically from the plots according to equation (1). See color version of this figure at back of this issue.

because photochemistry is weaker and the vortex undergoes a pronounced seasonal cycle.

[5] Other diagnostic measures of mixing have been used. Analyzing the composition of the lowermost stratosphere, *Ray et al.* [1999] estimate transport across the tropopause barrier and from higher altitudes into this region from local measurements of trace gases. Variable abundances of these species at the upper and lower boundaries of the considered domain induce large uncertainties in their results.

[6] Long-lived tracers in the stratosphere often form compact "canonical" correlations [e.g., *Kelly et al.*, 1989; *Plumb and Ko*, 1992; *Hall and Prather*, 1995]. The appearance of such compact correlations has been known since the pioneering works of *Ehhalt et al.* [1983] and *Mahlman et al.* [1986]. Anomalous points lying off the canonical correlation curves have led to the identification of "mixing lines" [*Thuburn and McIntyre*, 1997; *Waugh et al.*, 1997]. Such lines can form if a pair of tracers forms a curved correlation

and air masses lying on distinct points of the curve are brought into contact. *Plumb et al.* [2000] point out three difficulties that such a simple concept encounters: First, a part of mixing occurs locally in tracer space and does not involve the formation of mixing lines cutting across large tracts of otherwise sparsely populated areas of tracer space. Such local mixing may lead to a gradual change of tracer relationships [*Plumb and Ko*, 1992]. Second, the presence of multiple "canonical correlations" complicates the unambiguous construction of mixing lines; examples will be discussed in this paper. Finally, in many cases assuming only two points in tracer space as the origins of an observed air mass (which mixing lines really express) is insufficient; multiple origins must generally be assumed.

[7] *Morgenstern et al.* [2002] outline a method that aims to address the latter two of these problems. In a generalization of the concept of mixing lines, they propose that, in a mathematical sense, mixing constitutes a folding of isentropic tracer relationships, involving a folding kernel. This approach accounts for potentially broad distributions of origins in tracer space prior to a mixing event. Their method is however unsuitable to assess either local mixing (due to insufficient numerical sensitivity) or sustained mixing on a seasonal timescale because it does not take into account the impact of diabatic transport on tracer relationships on an isentropic surface.

[8] In the present paper we further develop the method of *Morgenstern et al.* [2002]. In particular, we aim to assess how a chemical transport model (CTM) captures mixing processes. We will apply two criteria to a CTM integration: First, we will examine in a global sense the extent to which the model generates compact canonical correlations of pairs of long-lived tracers which distinguish different well-mixed regions separated by transport barriers. To help establish the model in relation to other studies, in a digression we derive and discuss tracer lifetimes from the model simulation. Second, we will use an improved variant of the method detailed by *Morgenstern et al.* [2002] to investigate whether a change of the canonical correlations with time quantitatively reveals aspects of the air parcels' recent histories. *Morgenstern et al.* [2002] quantify mixing over a timescale of days, for which diabatic heating is unimportant. Here, however, the focus is on mixing on a timescale of months.

2. Chemical Transport Model

[9] The model data diagnosed in the following are taken from a CTM simulation using a variant of the SLIMCAT model described by *Chipperfield* [1999]. The model domain covers the region between 350 and 2800 K of potential temperature with 25 isentropic levels. (Due to model stability problems, in July 2000 the lower boundary is lifted to 362 K and the number of levels is reduced to 24.) The model simulates the evolution of 12 long-lived chemical tracers using a simplified chemistry described in Appendix A. The simulation at a resolution of 1.9° in latitude and longitude (T63) is initialized at 5 October 1999 from an earlier run; details are in Appendix B. The model uses climatological ozone fed into the MIDRAD middle atmosphere radiation scheme [*Shine*, 1987] to compute diabatic motion. Other meteorological data is taken from European Centre for Medium-Range Weather Forecasts (ECMWF) operational analyses, used at a resolution of 2.8° (T42). 25 of the 60 hybrid-pressure levels constituting the analyses reside at altitudes above 100 hPa; the top of the analysis domain is at 0.01 hPa. The model employs the *Prather* [1986] advection scheme which calculates second-order moments, effectively retaining memory of subgrid scales [*Hall and Prather*, 1995].

[10] CH_4 is the only long-lived tracer allowed to feed back into the abundances of the reactive radicals (Appendix A). Therefore, with the exception of CH_4 which influences the oxidizing capacity of the stratosphere, none of the following depends on the correct amplitudes and scaling of the trace gases, i.e., a proportional change of any tracer except CH_4 leaves the abundances of the other tracers and the diagnosis of mixing (section 4) unchanged.

3. Tracer-Tracer Correlations in the Model Runs

3.1. Meteorology of the Winters of 1999/2000 and 2000/2001

[11] The boreal winter of 1999/2000 saw an exceptionally strong, cold, and long-lived vortex with substantial ozone depletion [*Sinnhuber et al.*, 2000]. The vortex started to break up in mid-March although filaments and vortex fragments persisted until much later in spring. By contrast, in the winter of 2000/2001 the vortex was substantially weaker and more short-lived, and ozone depletion was less pronounced than in the year before.

3.2. Tracer Relationships

[12] To assess the model's performance in a global sense, we first examine correlative tracer plots. Figures 1 and 2 show the model's tracer-tracer relationships with N_2O in January 2000, and for CFC-11 throughout the integration period. (Chemical formulae relating to the technical names used in the following are listed in Table 1.) In Figure 1 the plot for 25 January 2000 is annotated with the labels "P", "ML", and "T", denoting the polar vortex, midlatitude and tropical canonical correlations of CFC-11 and N_2O that emerge from this plot. Similarly separated canonical correlations also appear in January 2001, and also for most of the other tracer relationships displayed in Figure 2. An exception is CFC-12 whose chemical lifetime is similar to N_2O. For CFC-11, CFC-12, CFC-113, CH_4, and halon-1211 the correlations are compared to the SAGE II Ozone Loss Validation Experiment (SOLVE) measurements taken during the winter of 1999/2000 [*Morgenstern et al.*, 2002]. For CFC-11, CFC-12, and CFC-113 the model is in good agreement with SOLVE observation, but the measurements presented there mainly cover the polar vortex only. The maximum (tropospheric) mixing ratio of CH_4 is slightly higher in the SOLVE observations than in the model. However, towards lower N_2O values CH_4 drops off more rapidly in the observations than in the model. Halon-1211 is likewise somewhat underestimated at the high-N_2O end but drops off more slowly than in the observations towards the low-N_2O end. These model problems are revisited in section 3.3 in the context of tracer lifetimes.

[13] *Avallone and Prather* [1997] discuss measurements covering all tracers calculated by our model, taken during the Airborne Arctic Stratospheric Expedition (AASE) II in the winter of 1991/1992. Broadly their measurements

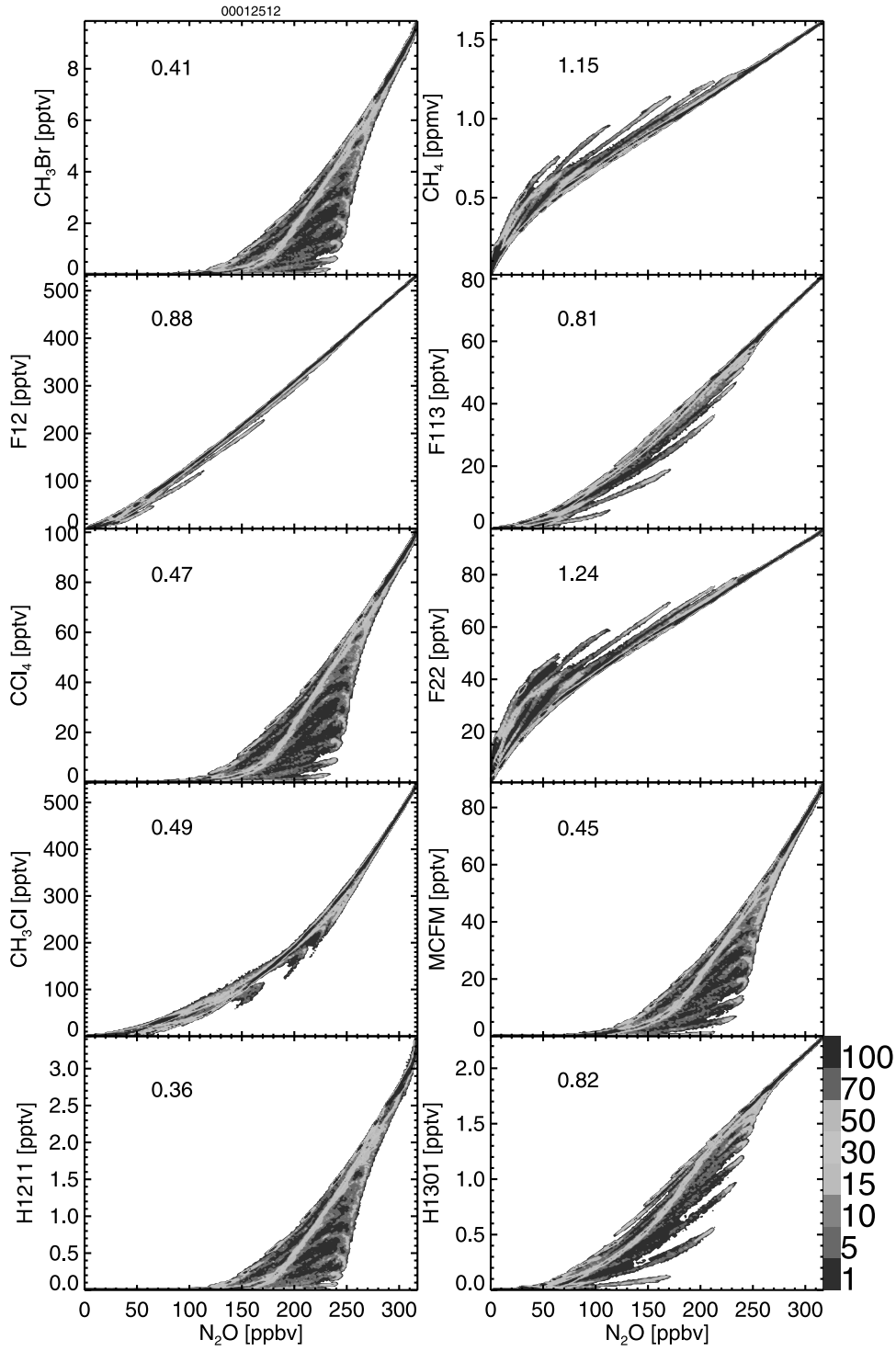

Figure 2. Same as Figure 1, but for the remaining model tracers. The displayed date is 25 January 2000, 1200 UTC. For CFC-11 see Figure 1. See color version of this figure at back of this issue.

resemble our model data, but the measurements do not form separate canonical curves. If that is not merely a display problem (*Avallone and Prather* [1997] present scatter rather than density plots), it is most likely caused by larger instrumental uncertainties than with newer measurements due to the use of a whole air sampler rather than a gas chromatograph during that campaign.

[14] For the midlatitude and tropical branches balloonborne data need to be considered. *Piani et al.* [2002] present a compilation of balloonborne measurements of CFC-11 versus N_2O, taken during the period 1996–2000, along with the SOLVE aircraft measurements. The measurements quoted there clearly show the existence of three separate canonical correlations in winter.

Table 1. Lifetime Calculations for the Model Species

Model Species	Lifetime[a]	Lifetime[b]	Lifetime[c]	Lifetime[d]	Lifetime[e]
N_2O	120	79–108	122 ± 24	106–175	120
CFC-12	106	69–95	87 ± 17	90–149	100
CFC-113	96	63–87	100 ± 32	55–101	85
Halon-1301	97	65–88		61–98	65
CFC-11	58	38–52	45 ± 7	35–68	45
CCl_4	56	36–49	32 ± 6	28–64	35
CFC-22	(148)	(96–131)			11.8
Halon-1211	(43)	(24–33)	24 ± 6	12–36	11
CH_4	(137)	(89–122)	23 ± 18		8.9
MCF	(54)	(34–47)	34 ± 7		4.8
CH_3Cl	(58)	(37–51)			1.3
CH_3Br	(49)	(31–42)			0.7

[a]Lifetimes τ_i assuming τ_{N_2O} = 120 years.
[b]Lifetimes τ_i assuming τ_{F11} = 45 ± 7 years.
[c]Measured lifetimes according to *Volk et al.* [1997], assuming τ_{F11} = 45 ± 7 years.
[d]Range of model lifetimes [*WMO*, 1999, Table 1–7].
[e]Recommended lifetime [*WMO*, 1999, Table 1–1]. F11 = $CFCl_3$, F12 = CF_2Cl_2, F113 = $CF_2ClCFCl_2$, F22 = CHF_2Cl, MCF = CH_3CCl_3, H1211 = CF_2ClBr, H1301 = CF_3Br. Equivalent lifetimes of hydrogenated species and halon-1211 are in brackets (see text).

[15] A comparison with the model results of *Avallone and Prather* [1997] indicates that their data do not support the existence of a separate polar vortex curve, and the tracers with the shortest lifetimes, halon-1211 and CH_3Br, exhibit tighter relationships with N_2O than the AASE II measurements to which they are compared. Note that their model resolution of 10° by 7.83° with 12 stratospheric layers is quite coarse, compared to ours. It is hence conceivable that these model problems of *Avallone and Prather* [1997] are caused by the low resolution employed in their model. A comparison of our tracer relationships with SLIMCAT model results at resolutions of 2.8° with 25 levels (T42L25) and at T63 with 12 levels indeed suggests that the separation of correlation functions critically depends on the high resolution both in the horizontal and vertical dimensions. In turn, for CFC-11/N_2O our model compares very well to that of *Piani et al.* [2002] who operate a variant of SLIMCAT similar to ours at a resolution of T106 (1.1°). This indicates that a further enhancement of the resolution will not qualitatively change the results. Our model improves on the results of *Avallone and Prather* [1997] by more accurately capturing features seen in the measurements.

[16] While the separation between the polar vortex and midlatitude curves is a seasonal feature restricted to winter and spring, that between midlatitudes and the tropics occurs year-round. However, the density of data points in the intermediate region differs considerably between summer and winter, suggesting that the exchange between the two regions peaks in summer, both in 2000 and 2001. The most striking difference between the two years relates to the breakdown phases of the polar vortices. Starting from similar initial conditions with separate polar canonical correlations appearing in midwinter, on 15 March 2000, the vortex has only just begun to get eroded, resulting in a sight increase in population density between the polar vortex and midlatitude curves. By contrast, in mid-March 2001, the two curves have entirely merged, creating a broad region of high population density. A comparison of isentropic maps of long-lived tracers (not shown) confirms that the vortex of 2000/2001 was a lot more unstable than that of the previous year, with the final warming already occurring in late February. This different evolution is visible throughout the spring period. At 1 June 2000, a well-defined midlatitude curve has formed. The somewhat diffuse nature of its inner side may result from the presence of some traces of identifiable former polar vortex air; this is the subject of section 4. Such a feature is not found in 2001; here, the broad midlatitude curve prevails at least until the end of May.

[17] Some model artifacts are also evident in Figures 1 and 2. One such artifact are the "fingers" appearing in the density plots between the tropical and midlatitude curves. This is a consequence of the discretization of levels and the choice of isentropic model levels. In Figure 1 for October 1999, the ''fingers'' are annotated with their corresponding potential temperature. The discretization of levels is also responsible for the intermittent nature of the polar vortex curves in the winter of 2000, evident in both Figures 1 and 2. Here, again high-density (dark) spots correspond to individual isentropic levels. Interestingly, in January 2001 such a behavior of the polar vortex curve is not evident, indicating that the interior of the vortex of 1999/2000 was more homogeneous and well mixed than that of 2000/2001. Note that in the T42 precursor simulation some tracers were initialized with simple polynomial fits to correlations with measured N_2O (Appendix B), hence no distinct correlations in different geographical regions were assumed. The deviations from such polynomial dependencies are therefore generated by the model.

3.3. Tracer Lifetimes

[18] Mixing in the lower stratosphere leads to the formation of linear relationships between sufficiently long-lived trace gases; Figures 1 and 2 show examples. The slopes of these relationships represent simple, unique, global, easily verifiable parameters by which to measure the performance of our model in relation to measurements and other models. *Plumb and Ko* [1992] establish a theory that links these linear correlations to tracer lifetimes according to

$$\frac{\tau_i}{\tau_j} = \frac{d\sigma_j}{d\sigma_i}\frac{\sigma_i}{\sigma_j}, \qquad (1)$$

where σ_i and σ_j are the tropospheric mixing ratios of two long-lived gases, τ_i and τ_j their respective lifetimes, and $d\sigma_j/d\sigma_i$ the linear correlation coefficient of the two species. Equation (1) holds for long-lived tracers whose local chemistry is slow compared to isentropic mixing at the altitude considered, have their source but no sink in the troposphere, and have a negligible long-term trend. Table 1 summarizes the resulting lifetimes and literature data. Assuming a reference lifetime of τ_{N_2O} = 120 years (as recommended by *WMO* [1999]), all resulting lifetimes but that of halon-1211 (Table 1a) fall within the ranges of lifetimes spanned by the various two- and three-dimensional CTMs compared in *WMO* [1999] (Table 1d) in so far as the species are discussed there. Halon-1211 experiences a substantial loss in the lowest model levels due to its comparatively long photodissociation wavelength [*Kaye et al.*, 1994]. This means equation (1) is inaccurate when applied to halon-1211, as may also be seen from

some curvature in the halon-1211-N_2O correlation at near-tropospheric mixing ratios of N_2O. The recommended lifetime of halon-1211 (Table 1e) is therefore somewhat smaller than that derived from the model, which includes only stratospheric loss, in line with the systematic differences between measured and modeled halon-1211 discussed in section 3.2.

[19] Comparing the model lifetimes to those derived from measurements by *Volk et al.* [1997] and assuming $\tau_{CFC\text{-}11} = 45 \pm 7$ years, again for most species the model lifetimes (with uncertainties stemming from the assumed uncertainty of CFC-11; Table 1b) overlap with the intervals of possible lifetimes derived from the measurements (Table 1c). Only the model lifetime of CH_4 lies outside the range of uncertainties, though for some species the model lifetimes are near the short (N_2O, MCF, halon-1301) or long (CCl_4) ends of the ranges of possibilities. The slope of the CFC-11-N_2O correlation is somewhat at odds with the ratio of their recommended lifetimes, suggesting either some uncertainty in deriving the slope from measurements, or model problems with the representation of their photochemistries or with diabatic transport. In the case of CH_4 it should be noted that losses via Cl and OH are of roughly the same importance as those via photolysis and $O(^1D)$, but Cl and OH are not as well captured by the model as $O(^1D)$ and photolysis. This may explain the relatively large problem with CH_4, compared to the other tracers. Note that in the presence of a long-term tropospheric trend equation (1) needs to be modified [*Volk et al.*, 1997]; this does however not apply to our model results because tropospheric long-term trends are neglected in the lower boundary condition.

[20] For N_2O, the chlorofluorocarbons (CFCs), and halon-1301 the model lifetimes are relatively close to the lifetimes recommended by *WMO* [1999] (Table 1e), but for the hydrogenated species order-of-magnitude differences occur. For these species the loss is dominated by reactions with OH in the troposphere. Since the model has no representation of tropospheric OH abundances (and includes only a fraction of the troposphere in its domain), the results represent ''equivalent'' stratospheric lifetimes. For MCF *Kaye et al.* [1994] obtain a stratospheric removal time of 45 years, which is close to our model result (Table 1b). Such equivalent lifetimes appear in brackets in Table 1 and do not correspond to residence times in the atmosphere.

[21] In the determination of mixing (section 4) a weighting of tracers is necessary (Appendix C). For N_2O, the CFCs, and halon-1301 the recommended lifetimes (Table 1e) are taken as weights. For halon-1211 and the hydrogenated species, for the reasons discussed above, these numbers do not reflect stratospheric chemical activities. For these compounds, we take the model equivalent lifetimes (Table 1a).

[22] The above allows us to infer that the model performs a realistic treatment of transport and chemistry of long-lived tracers in the stratosphere, following earlier validations of versions of the model [e.g., *Chipperfield*, 1999]. We proceed to assess whether model tracer-tracer correlations can be used to quantify long-range transport and mixing. We analyze two examples of vortex breakdown at the end of the boreal winter.

4. Detection of Polar Vortex Debris from Tracer-Tracer Correlations

4.1. Formalizing Stratospheric Transport and Mixing

[23] In a general approach the effect of transport and mixing in the atmosphere on a long-lived tracer can be described by

$$\psi_i(\mathbf{r}, t) = \iiint T_3(\mathbf{r}, t; \mathbf{r}_0, t_0)\psi_i(\mathbf{r}_0, t_0)\mathrm{d}^3 r_0, \qquad (2)$$

where ψ_i denotes the mixing ratio of the tracer, the triple integral extends over the entire atmosphere, and the three-dimensional transport operator T_3 describes the fraction of an air parcel at position $\mathbf{r}_0$ and reference time t_0 that ends up in the parcel at position $\mathbf{r}$ and time t. Chemical and other nonconservative processes are neglected in this formulation, i.e., the transport operator is nonnegative ($T_3 \geq 0$), and continuity imposes $\int\int\int T_3 \, \mathrm{d}^3 r_0 = 1$. If in a special case the composition of an air parcel remains unchanged under transport, then T_3 reduces to a δ-function.

[24] Long-lived tracers in the stratosphere usually exhibit tight ''isentropic correlations'' with a reference tracer ζ, for example N_2O [*Morgenstern et al.*, 2002]. Isentropic correlations are correlation functions obtained by sampling a tracer pair on an isentropic surface only, to be distinguished here from "canonical correlations". For most tracer pairs in Figures 1 and 2, the tropical, midlatitude and polar vortex canonical correlations appear as ridges in the density plots, indicating that the composition of much of the stratosphere is described by those three canonical correlations. In addition, on any of the isentropic (model) surfaces the composition falls on tight isentropic correlations. Following the notation of *Morgenstern et al.* [2002], let $\Psi_i(\zeta, \Theta, t_0)$ denote the isentropic correlation of ζ with the i-th tracer on the isentropic surface Θ at the reference time t_0, valid for one hemisphere. The transport integral equation (2) can then be approximated by

$$\psi_i(\mathbf{r}, t) \approx \iint T_2(\mathbf{r}, t; \zeta, \Theta, t_0)\Psi_i(\zeta, \Theta, t_0)\mathrm{d}\zeta \, \mathrm{d}\Theta. \qquad (3)$$

Here, T_2 denotes a two-dimensional transport operator. The reference tracer ζ replaces the horizontal coordinates of equation (2).

[25] If diabatic transport may be neglected, or if $t = t_0$, then equation (3) formally reduces to *Morgenstern et al.*'s [2002] equation (1). The transport operator T_2 satisfies $T_2 \geq 0$ and $\int\int T_2(\mathbf{r}, t; \zeta, \Theta, t_0) \, \mathrm{d}\zeta \, \mathrm{d}\Theta = 1$, expressing tracer continuity.

[26] Given p long-lived tracers, equation (3) may be inverted to yield an approximation to T_2. Individually at each grid point ($\mathbf{r}$, t) of the model run (section 2) the quadratic form

$$f(H; \mathbf{r}, t) = \left\| \psi(\mathbf{r}, t) - \iint H(\mathbf{r}, t; \zeta, \Theta, t_0)\Psi(\zeta, \Theta, t_0)\mathrm{d}\zeta \, \mathrm{d}\Theta \right\|^2 \qquad (4)$$

is minimized with respect to a family of test functions H approximating T_2. The functional f measures the squared

distance in tracer space between the composition of the atmosphere at a grid point and point of time and the composition that would be generated if transport and mixing were described by H. Here, $\psi(\mathbf{r}, t) = (\psi_1, \ldots, \psi_p)$ and $\Psi(\zeta, \Theta, t_0) = (\Psi_1, \ldots, \Psi_p)$ are the vector notations of the mixing ratios and isentropic correlations, and the norm $\|.\|$ measures distances in p-dimensional tracer space. The choice of norm (a 2-norm) is discussed in Appendix B. Note the similarity to *Morgenstern et al.*'s [2002] equation (2), but here the integral is extended to include a vertical dimension, and the isentropic correlations Ψ_i and atmospheric states ψ_i refer to different points of time, t and t_0. The test functions H are restricted to be piecewise uniform in m different regions of (ζ, Θ) space. As such H can then be expressed as a vector $H(\mathbf{r}, t) \sim (H_0, \ldots, H_{m-1})$, where the H_k denote the fractional contributions to the composition of the air mass at $(\mathbf{r}, t)$. By normalization the H_k satisfy $0 \leq H_k \leq 1$ and $\Sigma_k H_k = 1$. The m different partitions of (ζ, Θ) space are referred to as "bins", the H_k as "bin amplitudes". The minimization of $f(H)$ is then performed with respect to the bin amplitudes H_k. Formally this approach is similar to that of *Morgenstern et al.* [2002], but here it additionally accounts for diabatic motion and hence allows for cumulative effects of mixing to be examined. More details of the inversion procedure are in Appendix C. An example of the arrangement of bins in (ζ, Θ) space is displayed in Figure 3. Here, the horizontal bars denote the ranges of variability of ζ (N_2O) on the three isentropic surfaces considered in this study at time t_0, whereby low values of ζ correspond to the polar vortex and high values to the tropics. The vertical bars hence define a subdivision of the (northern) hemisphere into regions whose boundaries corresponding to contours of ζ. The mixing analysis will hence determine how large a fraction of an air parcel has originated in any of the displayed bins. Note that the spacing of bin boundaries is nonuniform in ζ. It is designed to yield an adequate resolution in middle and high latitudes.

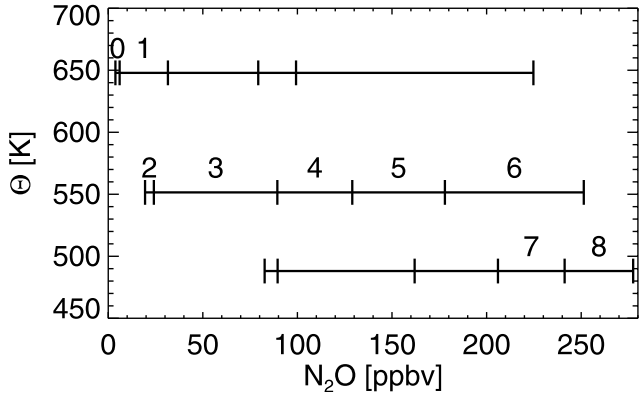

Figure 3. Position of bins in (Θ, ζ) space. The bin boundaries correspond to 90, 80, 65, 45, 25, and 0° of equivalent latitude at 7 March 2000, in the SLIMCAT T63L25 integration. The bins that are labelled with numbers 0–8 are assumed to contribute to the composition at the 551 K level during the period of analysis. The contributions of the others are assumed 0.

4.2. Case Study: Diagnosis of Mixing During Spring 2000

4.2.1. Vortex Evolution From Isentropic N_2O Maps

[27] Figure 4 displays N_2O on the 551 K isentropic surface for selected days of spring 2000. In early March the vortex is intact though elongated. By 27 March it has broken up into fragments of various sizes. The fragments eventually mix with the midlatitude intrusions to reform a weaker vortex. Subsequent successive filament shedding and dilution further erode the vortex. This period coincides with a change from westerlies to easterlies in the midlatitude surf zone. At 30 May some "fossil" vortex debris is still discernible over Siberia, and the remainder of the northern middle latitudes exhibits substantial structure in the N_2O field. Patches with N_2O mixing ratios characteristic of the polar vortex have disappeared by 21 June.

4.2.2. Diagnosis of Mixing From Tracer Relationships

[28] We apply the formalism outlined in section 4.1 to the period 7 March to 21 June 2000, with the arrangement of bins depicted in Figure 3. In Figure 5, the contribution H_0 denotes the fraction of air that has been in the core of the vortex at 648 K at 7 March 2000, while H_2 is the fraction that resided in the core at 551 K. The sum of both marks the fraction of air that was in the core of the vortex on 7 March 2000. Until mid April, the diagnosis suggests a considerable shrinkage of the polar vortex, at the expense of traces of former vortex air appearing throughout the middle latitudes. However, the core of the vortex remained largely uninfluenced by mixing with the vortex air fraction exceeding 80% in the center of the vortex. *Waugh et al.* [1997] find a similar behavior for the vortex of 1992/1993. By 10 May, dilution has appreciably changed the composition of the vortex core, although the vortex is still an easily distinguishable and compact entity. After 10 May, the vortex disappears, but the method finds a significant amount of vortex debris scattered around the middle latitudes. Much of the structure visible in the diagnosis of vortex debris is also evident from the isentropic maps of N_2O (Figure 4).

4.2.3. Direct Idealized Tracer Transport Experiment

[29] The diagnosis of mixing from tracer-tracer correlations depends, among other things, on the assumption that chemistry plays only a negligible role. Moreover, the numerical adequacy of the scheme outlined in section 4.1 needs to be examined. Hence to verify that the scheme indeed allows air masses to be traced, a direct idealized tracer transport experiment was performed. On 7 March 2000, an idealized tracer was set to 1 poleward of 70° of N_2O-equivalent latitude, and to 0 elsewhere. With this definition the patch of idealized tracer has roughly the same size and shape as the bin amplitudes $H_0 + H_2$ of Figure 5 at that date.

[30] The idealized tracer was then subjected to the same transport as the chemical tracers but did not experience any chemistry. Its resulting distributions for 10 May and 21 June 2000, are displayed in Figure 6. A comparison with Figure 5 suggests that the two experiments yield broadly the same results, though some differences occur in detail. In particular, the experiments agree that there is a 5 to 10% contribution of former polar vortex air throughout most of the extratropical Northern Hemisphere in late June with little export to the tropics. This is less than one could expect from a thought experiment in which a vortex bounded by 67° of latitude is mixed evenly into middle and high

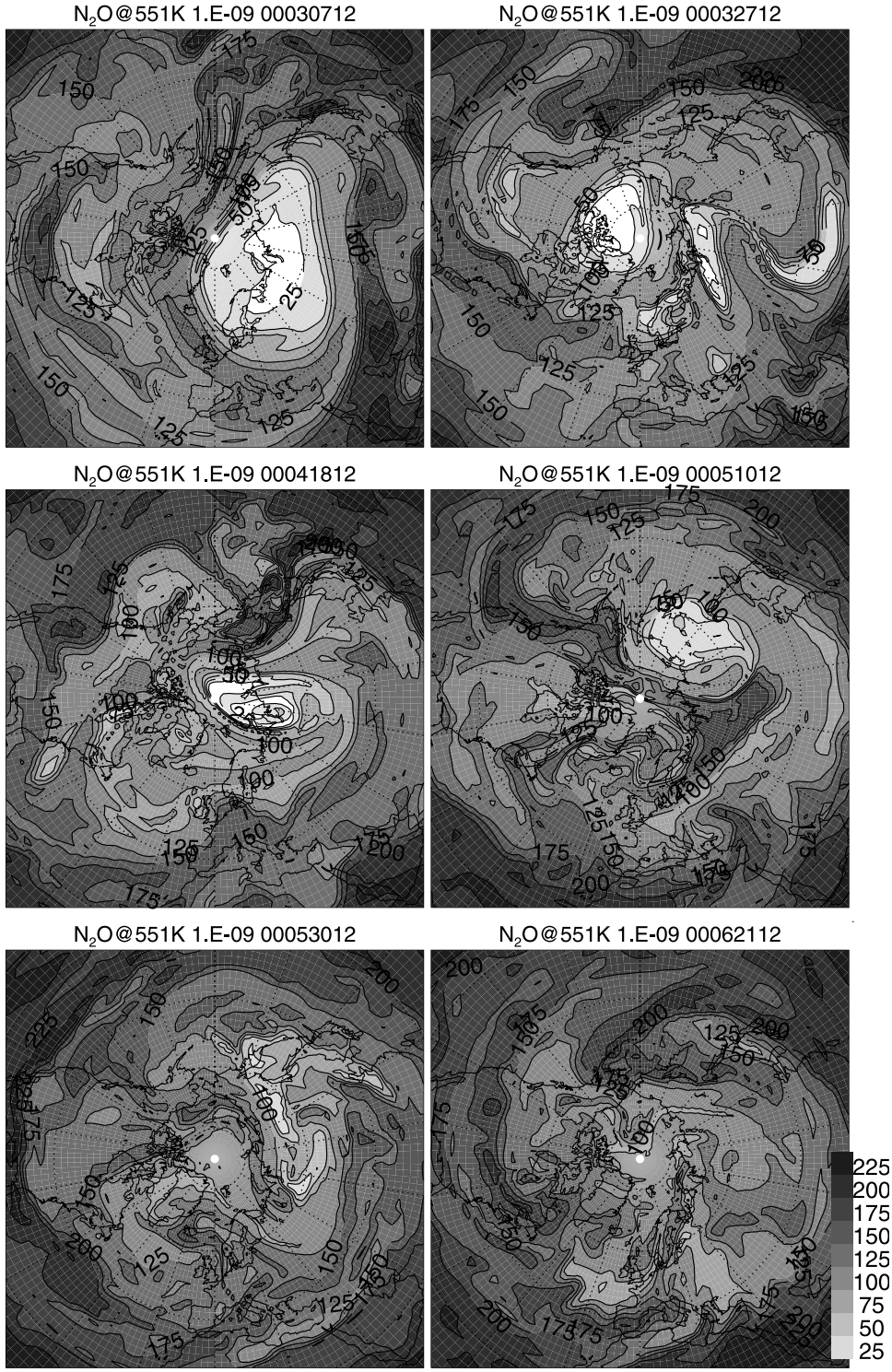

Figure 4. N_2O in ppbv at the 551 K surface, from 7 March to 21 June 2000, from the SLIMCAT T63L25 integration.

latitudes; this would yield an average vortex contribution of 16%. The discrepancy points to the three-dimensional nature of transport. *Piani et al.* [2002] observe a similar effect of the subtropical barrier on their ozone-loss tracer. On 10 May, both experiments show an intrusion of tropical or subtropical air extending across the North Pole. The vortex remnant over Eastern Siberia is likewise picked up by both calculations. At 21 June, both experiments reveal enhanced fractions of polar vortex air over Europe and the Eastern Atlantic with tongues extending along the Siberian Arctic coast and across Central Asia. For this feature, however, the highest concentrations of over 30% found in the tracer transport experiment are not reproduced in the mixing diagnosis. This and other differences are rooted in

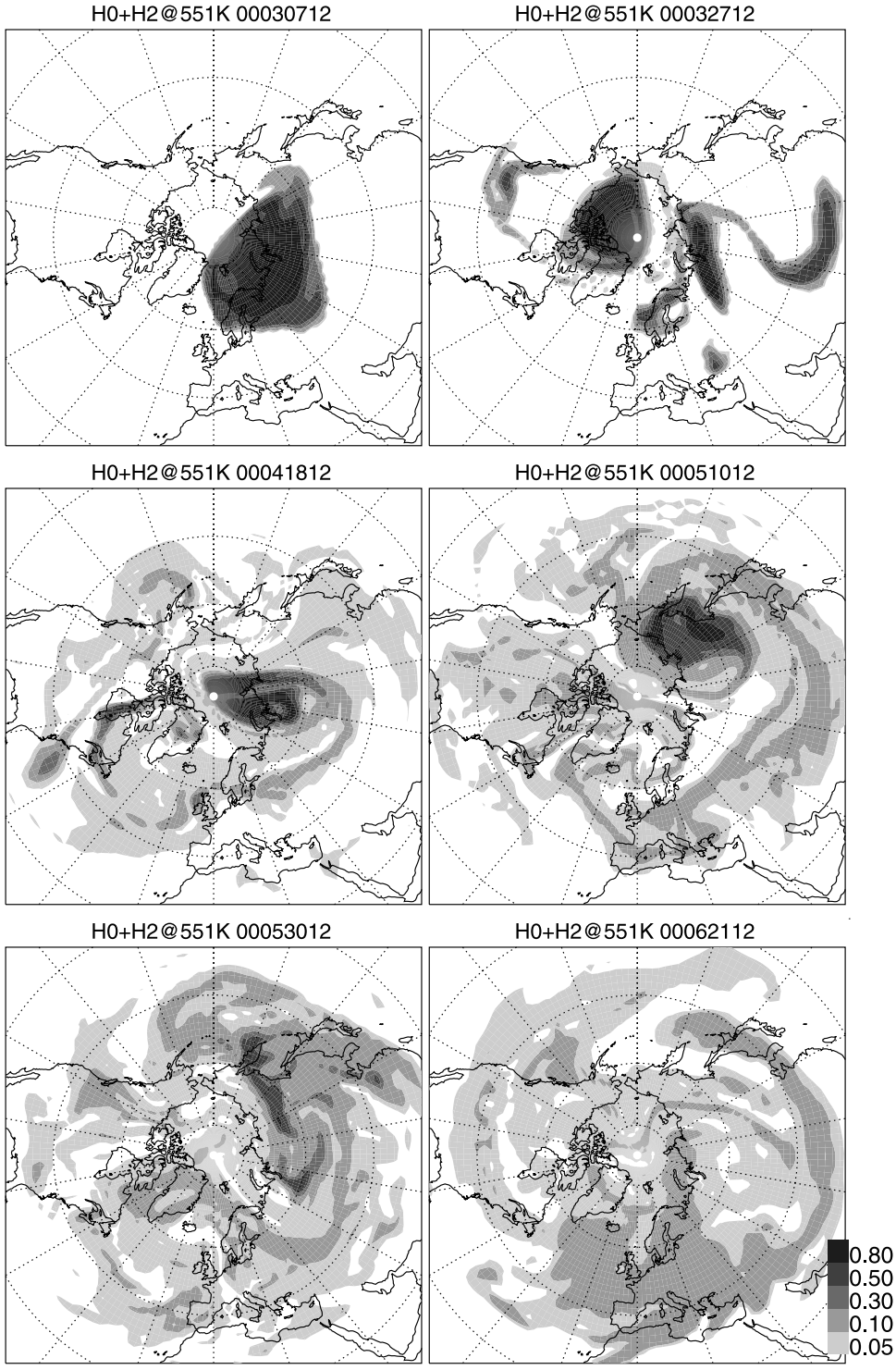

Figure 5. Fraction of core-vortex air, $h_0 + h_2$, at 551 K from 7 March to 21 June 2000.

the numerically coarse nature of the mixing diagnosis which is discussed in some detail in section 5.

4.3. Case Study: Vortex Breakdown in the Winter of 2000/2001

4.3.1. Mixing Diagnosis of the Vortex Breakdown of 2000/2001

[31] To illustrate the applicability of the method to different altitudes we choose to analyze the vortex breakdown of 2000/2001 at a lower isentropic level than for the previous winter (section 4.2), namely at 470 K. This winter offers some interesting differences in tracer relationships, compared to the previous winter (section 3.2). An important difference is the more inhomogeneous nature of the vortex, which within the framework of mixing diagnosis pursued here means that a larger number of bins than in 1999/2000 is needed to trace air from the vortex core. The positions of the bins are displayed in Figure 7. In contrast to the case of

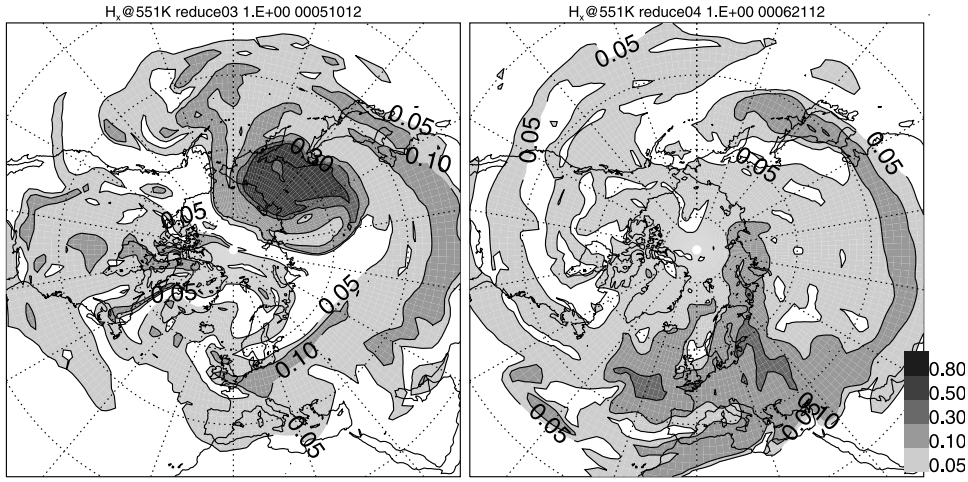

Figure 6. Fraction of polar vortex air at 551 K at (top) 10 May and (bottom) 21 June 2000, 1200 UTC (see section 4.2.3).

section 4.2, two bins per level (a total of four) are taken to cover the center of the polar vortex. Mixing is analyzed following 24 January 2001, the reference time t_0, starting from largely unperturbed conditions. The chosen bins allow us to account for isentropic transport on the 470 K surface, descent in the vortex core from the 530 K surface, and ascent in the tropics from the 417 K surface.

[32] With the arrangement of bins used here (Figure 7), the vortex core is described by the sum of the contributions H_k from the bins 0 to 3, i.e., $H_0 + H_1 + H_2 + H_3$. The result of the mixing diagnosis is displayed in Figure 8. On 24 January, the polar vortex is situated over the pole, and the edge of the vortex is relatively clearly defined. A comparison with the situation at the same date of the previous year (not shown) indicates that the vortex is substantially smaller in the year 2001, explaining the lower density of population along the polar vortex canonical correlation in the winter of 2001 (Figure 1).

[33] By 9 February, the vortex has gone through a wave-breaking cycle, is now elongated and has formed a cut-off system centered over Finland. Along much of the perimeter of the vortex, mixing ratios of polar vortex air have dropped below 0.8, indicating that some mixing has occurred with midlatitude air.

[34] By mid-March, the vortex is reduced to a few vortex fragments, the largest one over the Russian Far East. Note that for the previous year, though at a later time of the year, also a sizeable vortex fragment is found to linger in the same region (Figures 5 and 6). *Knudsen and Andersen* [2001] find that the large negative multiannual trend in springtime ozone over Eastern Siberia is explained mainly by ozone depletion in the vortex, suggesting that vortex fragments have a climatological predilection to linger in this area during spring. Traces of former vortex air are, however, found throughout much of the Northern middle and high latitudes. In total, as can be expected from the smaller size of the vortex in midwinter, in 2001 the traces are less abundant than in the previous year.

4.3.2. Idealized Tracer Advection Experiment for 2000/2001

[35] As for the year 1999/2000, an idealized tracer advection experiment is performed to verify that the structures found by the above analysis indeed constitute former polar vortex air. On 20 January a tracer is set to mark the region north of 70° of equivalent latitude. The distribution of the tracer during the course of the advection experiment is displayed in Figure 9. On 24 January, practically no mixing has occurred across the vortex boundary. On 9 February and 15 March, the patterns generated by the simple advection experiment resemble those from the mixing diagnosis, though again there are some differences in detail. For example, on 15 March the Siberian vortex remnant is less pronounced in the tracer advection study than in the mixing diagnosis. On the whole, however, the structure and amplitude of the vortex-core tracer mixing ratio suggest that indeed the mixing diagnosis approximately traces polar vortex air into spring.

5. Discussion

[36] The main part of the paper deals with introducing a methodology for the diagnosis of mixing and then applying it to results generated using a stratospheric long-lived tracer model. The methodology is similar to that described in *Morgenstern et al.* [2002] but accounts for diabatic motion.

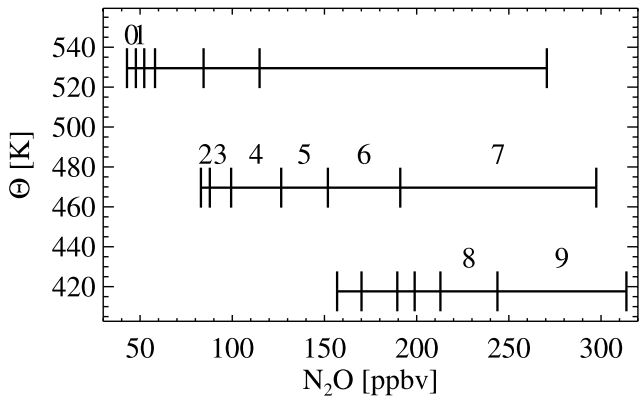

Figure 7. Positions of bins if (ζ, Θ) space for the diagnosis of vortex breakdown in the spring of 2001 (cf. Figure 3).

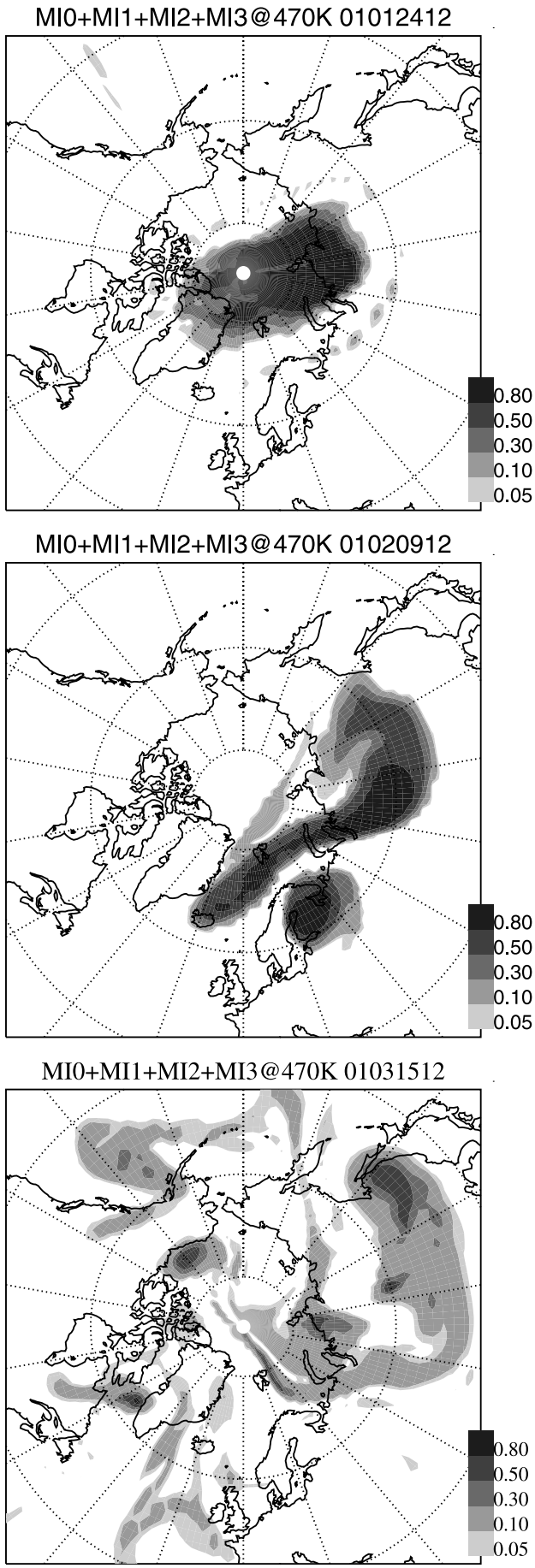

It is therefore applicable to the assessment of how mixing changes the distribution of trace species on a timescale of months. In contrast to *Morgenstern et al.* [2002], mixing is quantified which can be both local and long-range in tracer space [*Plumb et al.*, 2000]. Comparisons with experiments involving the plain advection of idealized tracers initially marking the polar vortex suggest that although there are differences in detail, the mixing diagnosis indeed picks out and quantifies traces of former vortex air at different stages of the vortex breakdown. The differences are partially rooted in the numerically coarse nature of the method, in particular the subdivision of (ζ, Θ) space into a small number of isentropic bins each representing a single, uniform region of origin of air. This approach hence fails to account for inhomogeneities within those bins. Instead of representing the "mixing kernel" T_2 by a piecewise constant approximation H, a continuous, piecewise linear (i.e., a linear spline) approximation has been tested. The results essentially verify the plots shown here. *Morgenstern et al.* [2002] discuss a corresponding study.

[37] Applicability of the mixing diagnosis as presented here depends on whether the chemical tracers can be assumed inert at the considered levels. Note that none of the chemical tracers studied here is strictly inert (Appendix A), though their local photochemical lifetimes need to be long compared to mixing timescales. Long-lived tracers such as N_2O and CH_4 better satisfy this condition than short-lived ones like halon-1211. It is therefore appropriate not to give all tracers equal weight in the introduction of the tracer norm (section 4.1), but to weigh them in proportion to their global atmospheric lifetimes (section 3.3), or, where global lifetime is determined by tropospheric processes, an "equivalent" stratospheric removal time. Lifetime is chosen mainly for simplicity; a sensitivity analysis shows that the results are only marginally different if, for example, equal weights are chosen. Also, in the lower stratosphere many tracers exhibit nearly linear relationships with each other. This could introduces a substantial amount of redundant information into the mixing analysis and is taken care of via an orthogonalization of tracer relationships (Appendix C).

[38] *Morgenstern et al.* [2002] apply a variant of the mixing diagnosis to measurements taken during the SOLVE/THESEO 2000 campaign. Essentially their analysis finds mixed air at the boundary of the vortex. An application of the mixing diagnosis presented here to measurements depends on whether at all and how accurately the considered measurements capture the canonical correlations. A variant of the method could be conceived that does not require knowledge of potential temperature, eliminating the need to consider isentropic correlations. A corresponding study is in progress to assess the suitability of measurement platforms and strategies for this particular problem. Assuming that our model simulation represents the real atmosphere and that observations differ from that through a random perturbation, then an error analysis could be conceived that is based on randomly perturbing the simulation

Figure 8. (opposite) Sum of bin amplitudes $H_0 + H_1 + H_2 + H_3$, at 470 K, for (top to bottom) 24 January, 9 February, and 15 March 2001, derived from tracer-tracer relationships of 24 January 2001 (see Figure 5).

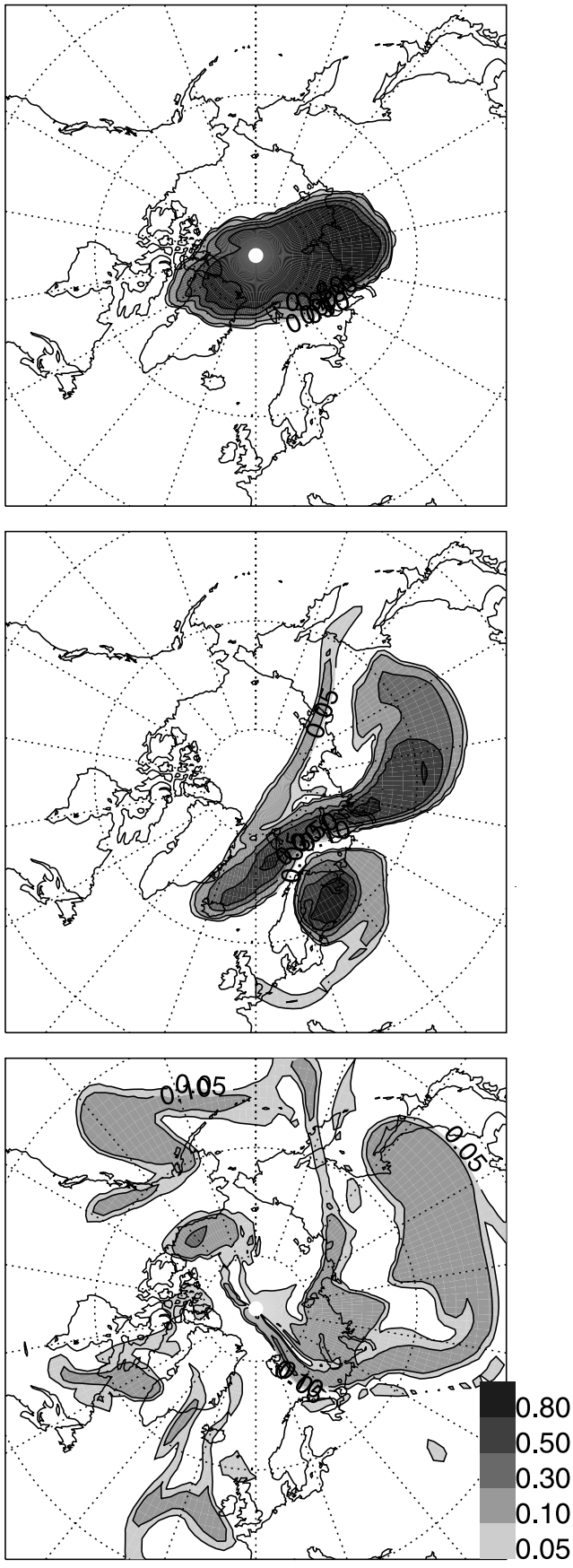

Figure 9. (oposite) Fraction of polar vortex air at 470 K, for (top to bottom) 24 January, 9 February, and 15 March 2001. See section 4.3.2 for explanation.

results with a fixed error distribution and then repeating the mixing diagnosis. Due to the heuristic nature of such an approach, some different error perturbations would need to be checked; this analysis is therefore postponed to future work.

[39] In a further application of the method, equation (3) can be applied to a short-lived tracer like ozone, NO_y, or water vapor, effectively amounting to subjecting the short-lived tracer to transport but not chemistry. The difference of the tracer distribution resulting from that projection and the actual, short-lived tracer then equals the chemical impact, with the effects of mixing accounted for. This might be used to quantitatively assess ozone recovery in the breakdown phase of the vortex. *Rex et al.* [1999] perform a similar analysis for NO_y, based on a mixing-line approach. Since the model used here does not transport any short-lived species, we have not performed this step, but when in due course full chemistry can be computed at a sufficient resolution, this becomes feasible. Also it could be applied to experimental data, for example future high-resolution satellite data.

[40] The model computes vertical motion using a radiative transfer mechanism based on prescribed climatological ozone. *Morgenstern et al.* [2002] (who perform a similar integration also employing climatological ozone) document systematic differences between measurements and model results for long-lived tracers such as N_2O in the core of the vortex. The most likely explanation for this problem is a systematic bias in heating rates, creating flawed rates of subsidence in the vortex. For the model based diagnosis of mixing presented here this is, however, considered to be of minor importance.

[41] Including the spin-up at T42, the model is integrated over a total period of about two years. The first assessment of mixing is performed after about one year of integration. A comparison of correlative tracer-tracer plots from the beginning of the simulation (Appendix B) and after one year (Figures 1 and 2) indicates that the tracers have undergone some substantial development in the intervening period. Possible transient effects due to long chemical relaxation times (exceeding one year) cannot be ruled out at this time, but are considered to be unimportant. A comparison with the study by *Piani et al.* [2002] indicates good agreement of the CFC-11-N_2O correlation both with respect to their model integration and regarding measurements. Note that their integration covers a longer period of time, including a cyclical spin-up, and is performed at a higher resolution. The CFC-11 lifetime derived from the lower-stratospheric correlation with N_2O in the spring of 2000 is practically identical to that of 2001, further corroborating the assertion that transient effects play a minor role in the integration.

[42] Regarding the tracer lifetimes, for the long-lived, nonhydrogenated species (i.e., CFC-11, CFC-12, CFC-113, halon-1301, and CCl_4) the lifetimes generally fall within the limits of uncertainty documented in the literature. The chemical activity of halon-1211 in the lower layers of the

model causes its correlation with N_2O to be curved. This means that equation (1) is inaccurate in determining its equivalent stratospheric lifetime; moreover, the model does not capture its tropospheric loss. For the hydrogenated species, equivalent lifetimes are obtained that would equal the actual lifetimes if tropospheric OH could be eliminated. This simply reflects the absence of tropospheric chemistry in the model. Comparisons to documented lifetimes are therefore almost meaningless in these cases unless these are also equivalent in the above sense. In the one case cited above [*Kaye et al.*, 1994], a good correspondence is achieved between the equivalent lifetime and the stratospheric removal time of MCF.

6. Summary

[43] We introduce a variant of the SLIMCAT stratospheric CTM which computes the evolution of 12 long-lived tracers. The model is integrated at a relatively high resolution over a total period of two years, starting in March 1999. In the boreal winters of 1999/2000 and 2000/2001, the model produces canonical correlations relating pairs of long-lived tracers which individually describe polar vortex, midlatitude, and tropical conditions. Linear relationships between pairs of tracers developing in the lower stratosphere are exploited to determine relative lifetimes of the long-lived species. For the nonhydrogenated species, except halon-1211, the lifetimes are within the uncertainties reported in the literature. For halon-1211, deviations are due to its photodissociation in the troposphere and lower stratosphere, making the method to determine the lifetimes of the other tracers unsuitable for halon-1211. The breakdown phases of the northern polar vortices are studied for the springs of 2000 and 2001. In both cases an erosion of the polar vortex leads to a merger of middle- and high-latitude canonical correlations. A methodology is defined that allows us to quantitatively follow the whereabouts of former polar vortex air during and after the breakdown of the vortex. In the two cases considered, the fraction of former vortex air found in the middle and high latitudes is determined solely from the evolution of tracer relationships. The findings are verified using advection experiments performed with idealized tracers initially marking the core of the vortex. While the method proves to be applicable to both springs, substantial meteorological differences appear between the two cases, with the extremely long-lived 1999/2000 vortex, producing vortex ''fossils'', and a relatively short-lived vortex in 2000/2001.

Appendix A: Chemical Module

[44] The model explicitly computes the evolution of the long-lived tracers CH_4, CH_3Cl, CH_3Br, MCF, CFC-22, N_2O, CFC-11, CFC-12, CFC-113, CCl_4, halon-1211, and halon-1301. All of these species undergo photolysis and oxidation by $O(^1D)$. The hydrogen-containing species CH_4, CH_3Cl, CH_3Br, MCF, and CFC-22 additionally react with OH. Finally, CH_4 is destroyed via a reaction with atomic Cl. Hence the radicals OH, $O(^1D)$, and Cl need to be diagnosed. Note that in the following reaction rates are those of *De More et al.* [1997] and *Sander et al.* [2000], and photolysis rates are computed as functions of solar zenith angle and climatological distributions of key absorbers (ozone, CO_2, water). O means $O(^3P)$.

1. In the case of $O(^1D)$ the reactions

$$\begin{aligned} O(^1D) + \{N_2, O_2\} &\rightarrow O + \{N_2, O_2\} \\ O_3 + h\nu &\rightarrow O_2 + \{O, O(^1D)\} \\ O + O_2 + M &\rightarrow O_3 + M \end{aligned} \tag{A1}$$

allow to infer $O(^1D)$ and O from a prescribed climatological ozone. Curly brackets denote different channels. This scheme and the rate and photolysis constants are the same as used by *Chipperfield* [1999].

2. The ratios $[HO_2]/[OH]$ and $[H]/[OH]$ are determined from the equilibrium conditions

$$\begin{aligned} OH + O_3 &\rightarrow HO_2 + O_2 \\ OH + \{O, CO, H_2\} &\rightarrow H + \{O_2, CO_2, H_2O\} \\ H + O_2 + M &\rightarrow HO_2 + M \\ H + O_3 &\rightarrow OH + O_2 \\ HO_2 + \{O, O_3\} &\rightarrow OH + \{O_2, 2O_2\} \end{aligned} \tag{A2}$$

This is similar but simplified, compared to *Chipperfield* [1999].

HO_x is calculated, assuming chemical equilibrium, from the reactions

$$\begin{aligned} \{CH_4, HCl, HO_2, OH\} + OH &\rightarrow H_2O + \{CH_3, Cl, O_2, O\} \\ HO_2 + H &\rightarrow \{H_2 + O_2, H_2O + O\} \\ \{H_2O, CH_4, H_2\} + O(^1D) &\rightarrow OH + \{OH, CH_3, H\} \\ \{H_2O, CH_4, HCl\} + h\nu &\rightarrow H + \{OH, CH_3, Cl\}. \end{aligned} \tag{A3}$$

3. For atomic chlorine (Cl) the equilibrium is assumed to be determined by

$$\begin{aligned} \{CH_4, H_2, HO_2\} + Cl &\rightarrow HCl + \{CH_3, H, O_2\} \\ HCl + \{OH, h\nu\} &\rightarrow Cl + \{H_2O, H\} \end{aligned} \tag{A4}$$

Throughout most of the domain the loss of Cl via CH_4 dominates. Losses via reactions with H_2 and HO_2 become important in the upper stratosphere. They have been included to stabilize model chlorine in methane-depleted upper stratospheric air.

[45] In the above, for HCl, H_2O, CO, H_2, and O_3 we make simplifying assumptions. O_3 (as mentioned) is assigned a zonally symmetric, seasonally varying climatology. For HCl we prescribe a profile linear in log p and approximating the midlatitude data given by *WMO* [1999]. H_2O is fixed at 6.5 ppmv$-2 \times CH_4$, so dehydration is neglected. CO and H_2 are assumed to be 10 and 500 ppbv, respectively, throughout the atmosphere.

[46] To assess systematic problems caused by this simplified chemistry we compare the first month of the spin-up integration covering March to April 1999, at T42L25 (Appendix B) with an equivalent simulation, using basically the same model and covering the same period of time at the same resolution, but with full chemistry (the same as by *Chipperfield* [1999]). Global-mean mixing ratios of OH, Cl, and CH_4, averaged over the 30 days of integration, are displayed in Figure 10. Differences for OH in the global mean are marginal, even though a more detailed comparison reveals somewhat different spatial distributions, e.g., features related to increased OH at sunrise which the simplified

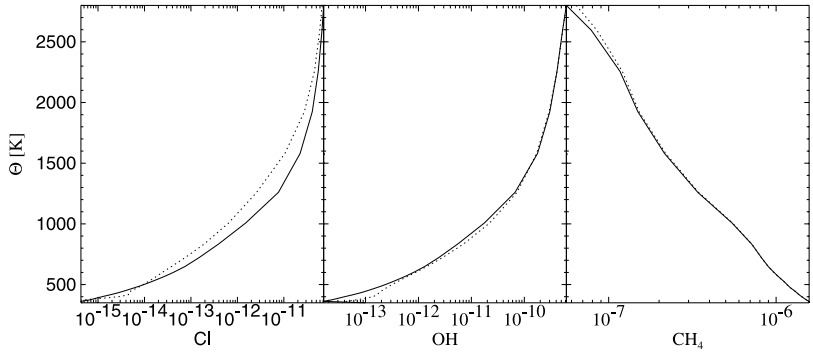

Figure 10. Global and monthly mean mixing ratio profiles of Cl, OH, and CH_4, for two simulations at T42 covering March/April 1999. Solid line: simplified chemistry. Dotted line: full chemistry. See text for explanations.

chemistry fails to reproduce. For the long-lived tracers, however, this is expected to play a minor role. For Cl somewhat larger differences occur, due to the important roles of $ClONO_2$ and ClO_x for the chlorine budget which the simplified chemistry does not include (section 5). CH_4, as expected, is practically the same throughout much of the domain, with the differences near the top probably due to the different rates of subsidence. (The full-chemistry integration used model ozone to compute vertical motion interactively.) With the exception of the five background fields as specified above, the chemistry is hence complete self-contained with no external information other than meteorology entering the chemical calculations.

Appendix B: Initialization of the Model Simulation

[47] First, a percursor simulation at a resolution of 2.8° (T42) with 25 levels is performed, covering the period from 5 March to 5 October 1999. This precursor simulation is driven with ECMWF analyses at a resolution of T42 with 50 analysis levels (L50), covering the entire period for which L50 analyses are available. To initialize this run, CH_4 and N_2O are taken from the T15L12 (7.5°) simulation described by *Chipperfield* [1999] and regridded to the T42L25 grid. CFC-11, CFC-12, CFC-113, and CCl_4 are initialized using correlations with N_2O measured by the ER-2 aircraft during the SOLVE/THESEO 2000 campaign. *Morgenstern et al.* [2002] partially reproduce the correlative data plots. Likewise, CFC-22 is initialized from a CFC-22-N_2O correlation measured during the AASE II campaign [*Wofsy et al.*, 1994]. CH_3Br is taken from the T15L12 integration, regridded, and rescaled such that its maximum mixing ratio equals 10 pptv, in accordance with *WMO* [1999] and *Schauffler et al.* [1999]. Halon-1211, CH_3Cl, and MCF are set proportional to CH_3Br such that their maximum mixing ratios equal 3.5 pptv, 550 pptv, and 90 pptv, respectively, likewise following *WMO* [1999]. Halon-1301 is set proportional to CFC-12 with a maximum mixing ratio of 2.3 pptv [*Schauffler et al.*, 1999]. Note that possible errors in the scaling of the fields have no effect on the mixing diagnosis presented in this paper. At the end of the precursor simulation all 12 long-lived tracer fields are regridded to 1.9° of resolution (T63L25).

Appendix C: Details of the Analysis of Mixing

[48] The mixing analysis is performed in a series of steps detailed in the following.

1. The isentropic correlation functions $\Psi_i(\zeta, \Theta, t_0)$ are determined for a given reference time t_0, in the two cases studied here 7 March 2000, and 24 January 2001. In contrast to *Morgenstern et al.* [2002], here regression and not envelope functions are taken as the background isentropic correlations. The interval of ζ values on every isentropic surface is subdivided into 100 equally sized subintervals, and $\Psi_i(\zeta, \Theta)$ taken to be the average of all points within those intervals. The different definition of the isentropic correlations reflects the change of focus from instantaneous to cumulative mixing.

2. Let $(\Theta_1, \ldots, \Theta_n)$ denote n neighboring isentropic model levels, for example the 480, 551, and 648 K levels. A function inner product $\langle \Phi, \Psi \rangle = \sum_{q=1}^{n} \int \Phi(\zeta, \Theta_q)\, \Psi(\zeta, \Theta_q)\, d\zeta$ is introduced (the sum replacing the integral in equation (4)). The Ψ_i (and the tracer fields ψ_i) are proportionally rescaled such that $\langle \Psi_i, \Psi_i \rangle = \tau_i^2$, where τ_i are the recommended atmospheric lifetimes listed in Table 1e. Where these do not reflect stratospheric chemical activity, the model lifetimes listed in Table 1a are taken (section 3.3).

3. The isentropic correlations $\Psi_i(\zeta, \Theta, t_0)$ are orthogonalized according to the prescriptions

$$\Psi_i' = \Psi_i - \sum_{j=0}^{i-1} \frac{\langle \Psi_i, \Psi_j' \rangle}{\langle \Psi_j', \Psi_j' \rangle} \Psi_j' \qquad \text{(C1)}$$

and accordingly the new "orthogonal tracers" become

$$\psi_i' = \psi_i - \sum_{j=0}^{i-1} \frac{\langle \Psi_i, \Psi_j' \rangle}{\langle \Psi_j', \Psi_j' \rangle} \psi_j' \qquad \text{(C2)}$$

at all model times. Note that the linear combination coefficients are the same for all points of time. Here $\Psi_0 = \psi_0 \equiv 1$ denotes the normalization "tracer", and $\Psi_1 \sim \zeta$ is the reference tracer (N_2O). The new tracer correlation functions satisfy $\langle \Psi_i', \Psi_j' \rangle = 0$ for $i \neq j$.

4. Let $s_k(\zeta, \Theta)$ for $k = 0, \ldots, m-1$ be a set of functions that are constant and nonzero on one isentropic surface and in one ζ interval only, and have non-overlapping, domain-filling supports (i.e., domains where they are nonzero). They are the equivalents of the nonoverlapping top-hat functions

of *Morgenstern et al.* [2002]. For 3 isentropic surfaces and 5 such intervals accordingly $m = 15$. Let the s_k be normed such that $\langle s_k, 1\rangle = 1$. Then a piecewise constant test function $H(\zeta, \Theta) = \sum_{k=0}^{m-1} H_k s_k\ (\zeta, \Theta)$ satisfies $\langle H, 1\rangle = \sum_{k=0}^{m-1} H_k$. A determination of the mixing operator involves minimizing $f(H_0, \ldots, H_{m-1})$ with respect to (H_k) at every grid point or for every measurement and at every point of time, subject to the conditions $\sum H_k = 1$ and $H_k \geq 0$.

5. Steps 1 to 4 define a projection of the p-dimensional vector field $\psi(\mathbf{r}, t) = (\psi_1, \ldots, \psi_p)$ onto the m-dimensional field of origins (or mixing kernel): $\psi \rightarrow (H_k)$. In the work of *Morgenstern et al.* [2002] the dimensionalities satisfy $p + 1 \geq m$, i.e., the minimization problem equation (4) is well posed. However, due to the two-dimensional nature of transport considered here, this is no longer the case. Nevertheless, in order to obtain a sensible solution, we note that trajectory studies, e.g., *Sparling et al.* [1997], indicate that certain pathways can be neglected, for example downward transport in the tropics and upward transport over the poles. In the present context this means that the corresponding "bin amplitudes" H_k that would represent such transport paths can be assumed zero. In our case, with 12 tracers and 15 original bins, technically only two such bins need to be assumed 0. Actually, as shown in Figures 3 and 7, further bins are neglected. The sensitivity to including individual excluded bins has been tested; their inclusion does not appreciably modify the results.

[49] Steps 1 to 4 are analogous to the one-dimensional problem outlined by *Morgenstern et al.* [2002]. The mathematical steps to define the solution are outlined there.

[50] **Acknowledgments.** Martyn Chipperfield is acknowledged for making both his model and the T15L12 simulation available. The British Atmospheric Data Centre is acknowledged for providing access to the UKMO and ECMWF analyses. OM is supported by the European Commission under grant EUK2-CT-1999-CO049 within the SAMMOA project. We acknowledge support by the U.K. Natural Environment Research Council (NERC) within the U.K. Universities Global Atmospheric Modelling Programme (UGAMP). The Centre for Atmospheric Science is a joint initiative of the Departments of Applied Mathematics and Theoretical Physics and of Chemistry.

References

Avallone, L. M., and M. J. Prather, Photochemical evolution in the lower tropical stratosphere, *J. Geophys. Res.*, *101*, 1457–1461, 1996.

Avallone, L. M., and M. J. Prather, Tracer-tracer correlations: Three-dimensional model simulations and comparisons to observations, *J. Geophys. Res.*, *102*, 19,233–19,246, 1997.

Chipperfield, M. P., Multiannual simulations with a three-dimensional chemical transport model, *J. Geophys. Res.*, *104*, 1782–1805, 1999.

De More, W. B., et al., Chemical kinetics and photochemical data for use in stratospheric modeling: Evaluation 12, *JPL Publ. 97-4*, 1997.

Ehhalt, D. H., E. P. Röth, and U. Schmidt, On the temporal variance of stratospheric trace gas concentrations, *J. Atm. Chem.*, *1*, 27–51, 1983.

Fahey, D. W., et al., A diagnostic for denitrification of the winter polar stratosphere, *Nature*, *345*, 698–702, 1990.

Goldan, P. D., W. C. Kuster, D. L. Albritton, and A. L. Schmeltekopf, Stratospheric $CFCl_3$, CF_2Cl_2, and N_2O height profile measurements at several latitudes, *J. Geophys. Res.*, *85*, 413–423, 1980.

Hall, T. M., and M. J. Prather, Seasonal evolutions of N_2O, O_3, and CO_2: Three-dimensional simulations of stratospheric correlations, *J. Geophys. Res.*, *100*, 16,699–16,720, 1995.

Hess, P. G., Mixing processes following the final stratospheric warming, *J. Atmos. Sci.*, *48*, 1625–1642, 1991.

Kaye, J. A., et al., Report on concentrations, lifetimes, and trends of CFCs, halons, and related species, *NASA Ref. Publ., 1339*, 1994.

Kelly, K. K., et al., Dehydration in the lower Antarctic stratosphere during late winter and spring, 1987, *J. Geophys. Res.*, *94*, 11,317–11,357, 1989.

Knudsen, B. M., and S. B. Andersen, Longitudinal variations in springtime ozone trends, *Nature*, *413*, 699–700, 2001.

Knudsen, B. M., and J.-U. Grooß, Northern midlatitude ozone dilution in spring modeled with simulated mixing, *J. Geophys. Res.*, *105*, 6885–6890, 2000.

Mahlman, J. D., H. Levy, and W. J. Moxim, Three-dimensional simulations of stratospheric N_2O: Predictions for other trace constituents, *J. Geophys. Res.*, *91*, 2687–2707, 1986.

Michelsen, H. A., et al., Intercomparison of ATMOS, SAGE II, and ER-2 observations in Arctic vortex and extra-vortex air masses during spring 1993, *Geophys. Res. Lett.*, *26*, 291–294, 1999.

Millard, G. A., A. E. Lee, and J. A. Pyle, A model study of the connection between polar and middle latitude ozone loss in the Northern Hemisphere lower stratosphere, *J. Geophys.*, *107*, doi:10.1029/2001JD000899, in press, 2002.

Minschwaner, K., A. E. Dessler, J. W. Elkins, C. M. Volk, D. W. Fahey, M. Loewenstein, J. R. Podolske, A. E. Roche, and K. R. Chan, Bulk isentropic properties of mixing into the tropics in the lower stratosphere, *J. Geophys. Res.*, *101*, 9433–9439, 1996.

Morgenstern, O., J. A. Pyle, A. Iwi, W. A. Norton, J. W. Elkins, D. F. Hurst, and P. A. Romashkin, Diagnosis of mixing between middle latitudes and the polar vortex from tracer-tracer correlations, *J. Geophys. Res.*, *107*(D17), 4321, doi:10.1029/2001JD001224, 2002.

Müller, R., P. J. Crutzen, J.-U. Grooß, C. Brühl, J. M. Russell, and A. F. Tuck, Chlorine activation and ozone depletion in the Arctic vortex: Observations by the Halogen Occultation Experiment on the Upper Atmosphere Research Satellite, *J. Geophys. Res.*, *101*, 12,531–12,554, 1996.

Müller, R., U. Schmidt, A. Engel, D. S. McKenna, and M. H. Proffitt, The O_3-N_2O relation from balloon-borne observations as a measure of Arctic ozone loss in 1991/92, *Q. J. R. Meteorol. Soc.*, *127*, 1389–1412, 2001.

Murphy, D. M., D. W. Fahey, M. H. Proffitt, C. S. Liu, K. R. Chan, C. S. Eubank, S. R. Kawa, and K. K. Kelly, Reactive nitrogen and its correlation with ozone in the lower stratosphere and upper troposphere, *J. Geophys. Res.*, *98*, 8751–8773, 1993.

Newman, P. A., et al., Measurements of polar vortex air in the midlatitudes, *J. Geophys. Res.*, *101*, 12,879–12,891, 1996.

Piani, C., W. A. Norton, A. M. Iwi, E. A. Ray, and J. W. Elkins, Transport of ozone depleted air on breakup of the stratospheric polar vortex in spring/summer 2000, *J. Geophys. Res.*, *107*(D20), 8270, doi:10.1029/2001JD000488, 2002.

Plumb, R. A., A "tropical pipe" model of stratospheric transport, *J. Geophys. Res.*, *101*, 3957–3972, 1996.

Plumb, R. A., and M. K. W. Ko, Interrelationships between mixing ratios of long-lived stratospheric constituents, *J. Geophys. Res.*, *97*, 10,145–10,156, 1992.

Plumb, R. A., D. W. Waugh, and M. P. Chipperfield, The effects of mixing on tracer relationships in the polar vortices, *J. Geophys. Res.*, *105*, 10,047–10,062, 2000.

Prather, M. J., Numerical advection by conservation of second-order moments, *J. Geophys. Res.*, *91*, 6671–6681, 1986.

Proffitt, M. H., et al., In situ ozone measurements within the 1987 Antarctic ozone hole from a high-altitude ER-2 aircraft, *J. Geophys. Res.*, *94*, 16,547–16,555, 1989.

Proffitt, M. H., J. J. Margitan, K. K. Kelly, M. Loewenstein, J. R. Podolske, and K. R. Chan, Ozone loss in the Arctic polar vortex inferred from high-altitude aircraft measurements, *Nature*, *347*, 31–36, 1990.

Pyle, J. A., M. P. Chipperfield, I. Kilbane-Dawe, A. M. Lee, R. M. Stimpfle, D. Kohn, W. Renger, and J. W. Waters, Early modelling results from the SESAME and ASHOE campaigns, *Faraday Discuss.*, *100*, 371–387, 1995.

Ray, E. A., F. L. Moore, J. W. Elkins, G. S. Dutton, D. W. Fahey, H. Vömel, S. J. Oltmans, and K. H. Rosenlof, Transport into the Northern Hemisphere lowermost stratosphere revealed by in situ tracer measurements, *J. Geophys. Res.*, *104*, 26,565–26,580, 1999.

Ray, E. A., F. L. Moore, J. W. Elkins, D. F. Hurst, P. A. Romashkin, G. S. Dutton, and D. W. Fahey, Descent and mixing in the 1999/2000 northern polar vortex inferred from in situ tracer measurements, *J. Geophys. Res.*, *107*(D20), 8285, doi:10.1029/2001JD000961, 2002.

Rex, M., et al., Subsidence, mixing, and denitrification of Arctic polar air measured during POLARIS, *J. Geophys. Res.*, *104*, 26,611–26,623, 1999.

Sander, S. P., et al., Chemical kinetics and photochemical data for use in stratospheric modeling: Evaluation 13, *JPL Publ. 00-3*, 2000.

Schauffler, S. M., E. L. Atlas, D. R. Blake, F. Flocke, R. A. Lueb, J. M. Lee-Taylor, V. Stroud, and W. Travnicek, Distributions of brominated organic compounds in the troposphere and lower stratosphere, *J. Geophys. Res.*, *104*, 21,513–21,535, 1999.

Shine, K. P., The middle atmosphere in the absence of dynamical heat fluxes, *Q. J. R. Meteorol. Soc.*, *113*, 603–633, 1987.

Sinnhuber, B. M., et al., Large loss of total ozone during the Arctic winter of 1999/2000, *Geophys. Res. Lett.*, *27*, 3473–3476, 2000.

Sparling, L. C., J. A. Kettleborough, P. H. Haynes, M. E. McIntyre, J. E. Rosenfield, M. R. Schoeberl, and P. A. Newman, Diabatic cross-isentropic dispersion in the lower stratosphere, *J. Geophys. Res.*, *102*, 25,817–25,829, 1997.

Thuburn, J., and M. E. McIntyre, Numerical advection schemes, cross-isentropic walks, and correlations between chemical species, *J. Geophys. Res.*, *102*, 6775–6797, 1997.

Tuck, A. F., et al., Polar stratospheric cloud processed air and potential vorticity in the Northern Hemisphere lower stratosphere at midlatitudes, *J. Geophys. Res.*, *97*, 7883–7904, 1992.

Volk, C. M., et al., Quantifying transport between the tropical and mid-latitude lower stratosphere, *Science*, *272*, 1763–1768, 1996.

Volk, C. M., J. W. Elkins, D. W. Fahey, G. S. Dutton, J. M. Gilligan, M. Loewenstein, J. R. Podolske, K. R. Chan, and M. R. Gunson, Evaluation of source gas lifetimes from stratospheric observations, *J. Geophys. Res.*, *102*, 25,543–25,564, 1997.

Waugh, D. A., et al., Mixing of polar vortex air into middle latitudes as revealed by tracer-tracer scatterplots, *J. Geophys. Res.*, *102*, 13,113–13,134, 1997.

Wofsy, S. C., R. C. Cohen, and A. L. Schmeltekopf, Overview-The Stratospheric Photochemistry Aerosols and Dynamics Expedition (SPADE) and Airborne Arctic Stratospheric Expedition-II (AASE-II), *Geophys. Res. Lett.*, *21*, 2535–2538, 1994.

World Meteorological Organization (WMO), *Scientific Assessment of Ozone Depletion: 1998, Rep. 44*, Global Monit. Prog., Geneva, 1999.

A. M. Lee and J. A. Pyle, Centre for Atmospheric Science, Chemistry Department, Cambridge University, Lensfield Road, Cambridge CB2 1EW, UK. (adrian.lee@atm.ch.cam.ac.uk; john.pyle@atm.ch.cam.ac.uk)

O. Morgenstern, Max-Planck-Institut für Meteorologie, Bundesstraße 55, D-20146 Hamburg, Germany. (morgenstern@dkrz.de)

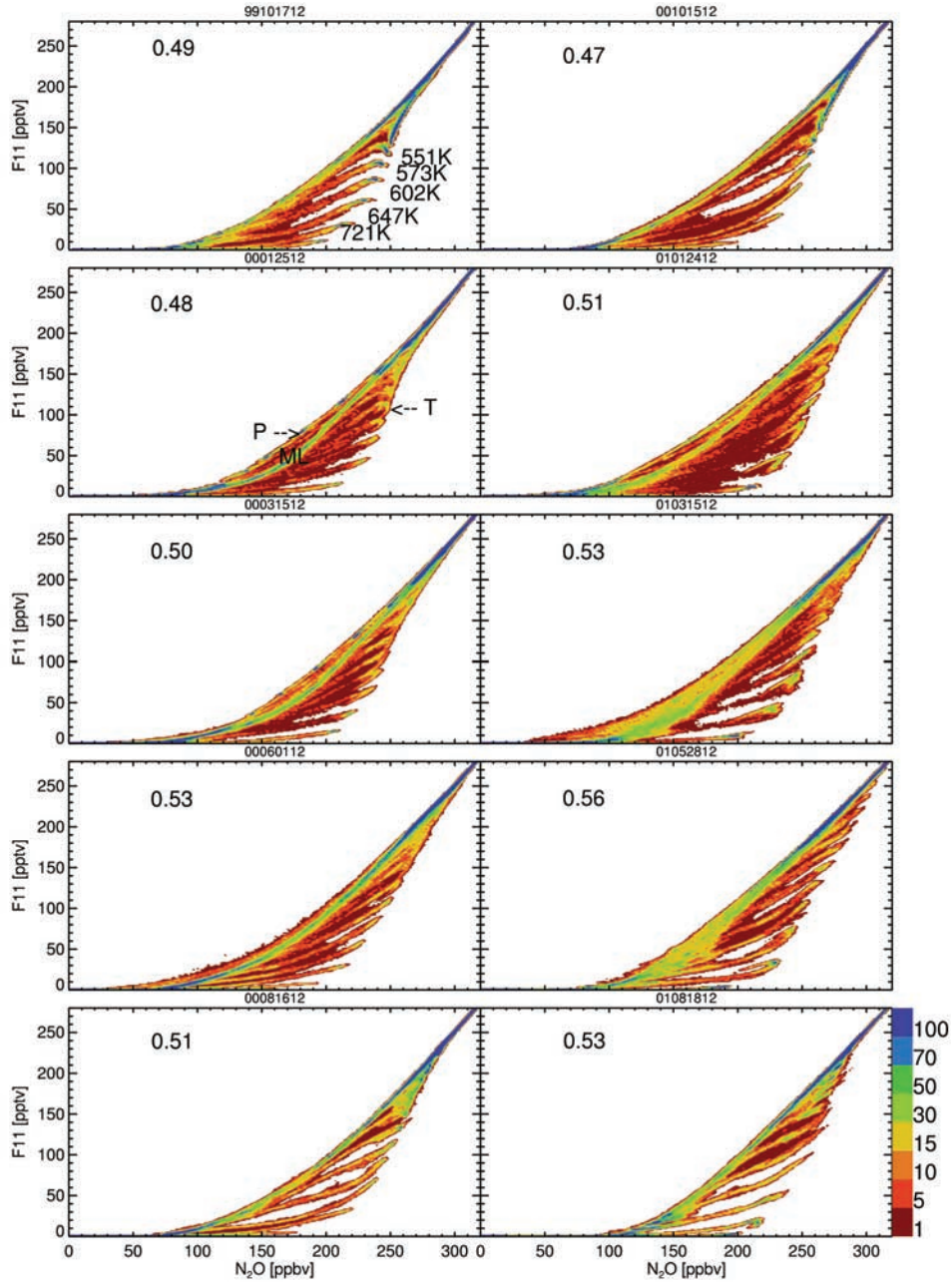

Figure 1. Density scatterplots of CFC-11 versus N_2O. Displayed dates are (left) 17 October 1999, 25 January, 15 March, 1 June and 16 August 2000; (right) 15 October 2000, 24 January, 15 March, 28 May, and 18 August 2001, all 1200 UTC. The displayed parameter space is divided into 200 × 200 equal-sized cells and the number of model grid points falling into each cell is counted. The bottom-boundary level at 350 K (362 K after July 2000) and Southern Hemisphere grid points are excluded. The numbers in the top left corners of the plots are $\tau_{CFC-11}/\tau_{N_2O}$, derived geometrically from the plots according to equation (1).

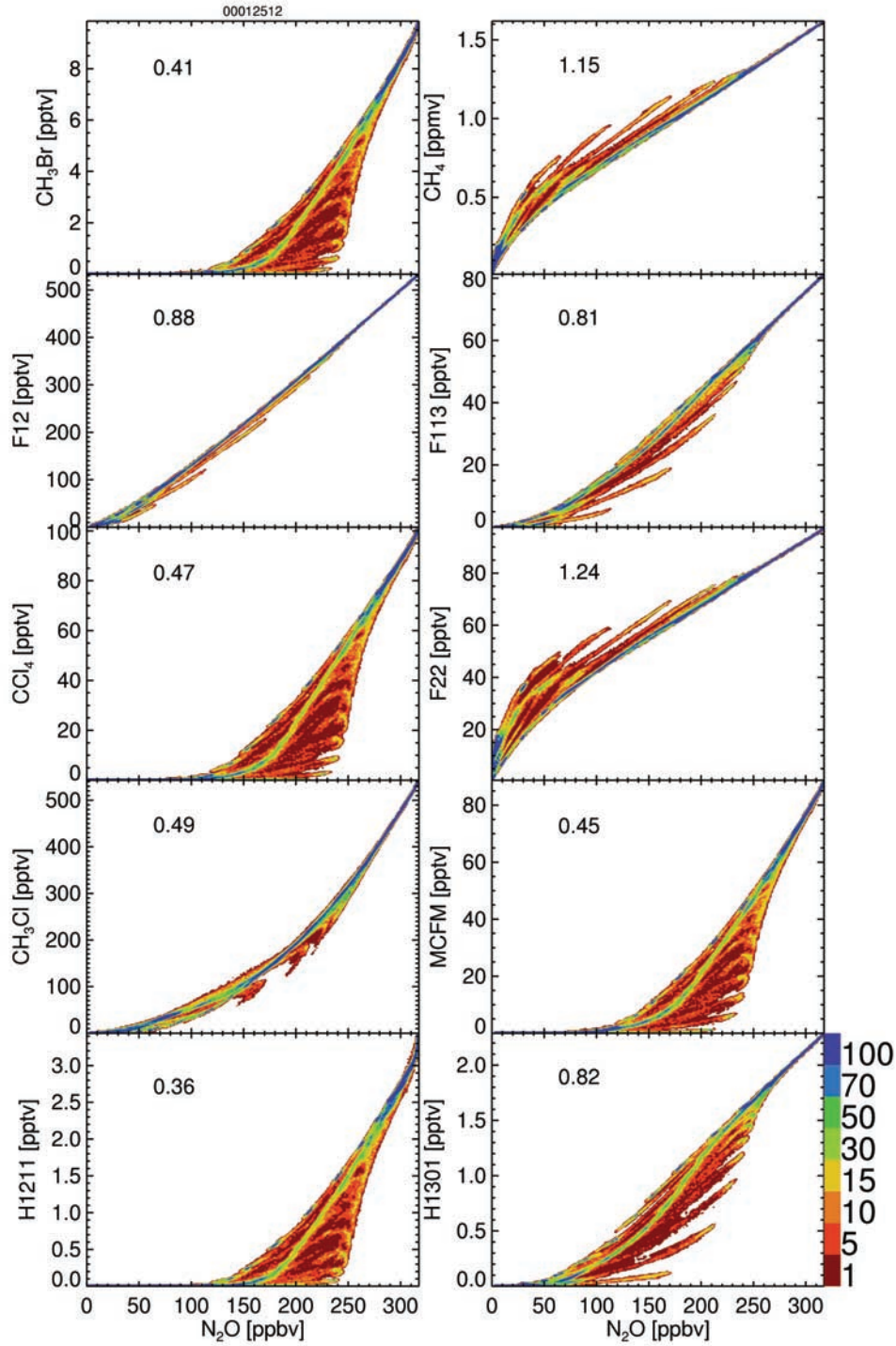

Figure 2. Same as Figure 1, but for the remaining model tracers. The displayed date is 25 January 2000, 1200 UTC. For CFC-11 see Figure 1.